

1 **Frequency-specific coactivation patterns in resting-state and their alterations in**
2 **schizophrenia: an fMRI study**

3

4 Hang Yang¹, Hong Zhang¹, Xin Di^{1,2}, Shuai Wang³, Chun Meng^{1*}, Lin Tian^{3*}, Bharat
5 Biswal^{1,2*}

6

7 ¹ The Clinical Hospital of Chengdu Brain Science Institute, MOE Key Laboratory for
8 Neuroinformation, Center for Information in Medicine, School of Life Science and
9 Technology, University of Electronic Science and Technology of China, Chengdu
10 611731, China.

11 ² Department of Biomedical Engineering, New Jersey Institute of Technology, Newark,
12 NJ, 07102, USA.

13 ³ Department of Psychiatry, The Affiliated Wuxi Mental Health Center of Nanjing
14 Medical University, Wuxi 214151, China

15

16 *** Correspondence:**

17 Dr. Chun Meng, The Clinical Hospital of Chengdu Brain Science Institute, MOE
18 Key Laboratory for Neuroinformation, Center for Information in Medicine, School of
19 Life Science and Technology, University of Electronic Science and Technology of
20 China, No. 2006, Xiyuan Avenue, Chengdu 611731, China; E-mail:
21 chunmeng@uestc.edu.cn

22 Dr. Lin Tian, Department of Psychiatry, The Affiliated Wuxi Mental Health Center
23 of Nanjing Medical University, No. 156 Qianhu Road, Binhu District, Wuxi 214151,
24 China; E-mail: tianz@njmu.edu.cn

25 Dr. Bharat B. Biswal, 607 Fenster Hall, University Height, Newark, NJ, 07102, USA;
26 E-mail: bbiswal@gmail.com

27

28 **Abstract**

29 The resting-state human brain is a dynamic system that shows frequency-specific
30 characteristics. Coactivation pattern (CAP) analysis has been recently used to identify
31 recurring brain states sharing similar coactivation configurations. However, whether
32 and how CAPs differ across different sub-frequency bands are unknown. In the current
33 study, in addition to the typical low-frequency range (0.01 - 0.08 Hz), the spatial and
34 temporal characteristics of CAPs in four sub-frequency bands, slow-5 (0.01 - 0.027 Hz),
35 slow-4 (0.027 - 0.073 Hz), slow-3 (0.073 - 0.198 Hz), and slow-2 (0.198 - 0.25 Hz),
36 were studied. Six CAP states were obtained for each band., The CAPs from the typical
37 frequency range were spatially largely overlapped with those in slow-5, slow-4 and
38 slow-3 but not with those in slow-2. With the increase of frequency, the CAP state
39 became more unstable and resulted in an overall shorter persistence. The spatial and
40 temporal characteristics of slow-4 and slow-5 were further compared, because they
41 constitute most power of the resting-state fMRI signals. In general, slow-4 showed
42 stronger coactivations or co-deactivations in subcortical regions, while slow-5 showed
43 stronger coactivations or co-deactivations in large-scale cortical networks such as the
44 dorsal attention network. Lastly, frequency-dependent dynamic alterations were also
45 observed in schizophrenia patients. Combining the information obtained from both
46 slow-5 and slow-4 increased the classification accuracy of schizophrenia patients than
47 only using the typical range. In conclusion, our results revealed that the spatial and
48 temporal characteristics of CAP state varied at different frequency bands, which could
49 be helpful for identifying brain alterations in schizophrenia.

50

51 **Keywords:** co-activation patterns, dynamics, frequency-specific, schizophrenia

52

53 **1. Introduction**

54 The human brain is a dynamic system, and the resting-state functional
55 connectivity (RSFC) has been proved to be temporally varied (Chang and Glover
56 2010). The conventional dynamic functional connectivity (dFC) approach segments

57 the time-series using sliding-window and calculates the interregional Pearson
58 correlation within each window (Chang and Glover 2010; Hutchison et al. 2013).
59 Moreover, recurring connectivity configurations across windows could be grouped as
60 FC-states (Allen et al. 2014). These FC-states were found to be related to cognitive
61 and physiological states such as vigilance (Wang, Ong, et al. 2016), self-generated
62 thought (Marusak et al. 2017), eyes open and closed (Weng et al. 2020), and also
63 disease alterations (Guo et al. 2019; Li, Dong, et al. 2020; Damaraju et al. 2014).
64 However, the choice of window length and window shape remained to be optimized
65 (Zalesky and Breakspear 2015; Shakil, Lee, and Keilholz 2016), and the temporal
66 resolution is also relatively low as the recommended window length is about 30-50
67 seconds (Hutchison et al. 2013).

68 Instead of estimating brain states using the sliding-window dFC maps, brain
69 states can also be identified based on recurring coactivation patterns (CAPs) from
70 each single frame (Liu and Duyn 2013). The CAP analysis was first performed using
71 a seed-based approach and a threshold was needed to select the suprathreshold frames
72 (Liu and Duyn 2013), then it was extended to a seed-and-threshold-free approach
73 (Liu, Chang, and Duyn 2013). Comparing with sliding-window dFC maps, CAPs are
74 more direct measurements of brain activities without any statistic or mathematic
75 calculation. It also has a better temporal resolution and does not require predefined
76 parameters such as window length, as the analytical unit of CAP analysis is a single
77 volume. Besides, our previous study has shown the robustness of CAPs across several
78 technique flexibilities and independent cohorts, and reproducible alterations were also
79 obtained between schizophrenia patients and healthy controls (Yang et al. 2021).
80 Recently, CAP analysis has been used to study the altered brain dynamics in patients
81 with depression (Kaiser et al. 2019) and Alzheimer's disease (Ma et al. 2020). In
82 addition, Li and colleagues concatenated a set of task activation maps from the
83 Human Connectome Project, and they identified robust anti-correlated functional
84 networks (default network) across multiple tasks (Li, Dahmani, et al. 2020),
85 suggesting that CAP analysis could also be utilized in task fMRI.

86 Besides the temporal dynamics contained in the resting-state fMRI blood oxygen
87 level dependent (BOLD) signals, frequency-dependent information also exists.
88 Previous resting-state fMRI studies mainly focused on the low-frequency oscillation
89 (LFO) which fluctuates at the typical low-frequency band (0.01 – 0.08/0.1 Hz), as the
90 LFO is thought to reflect the intrinsic neuronal fluctuations (Biswal et al. 1995).
91 Although the higher frequency fluctuations are regarded as physiological noise such
92 as respiration-induced and cardiac noise (Cordes et al. 2001), RSFC above 0.1 Hz and
93 the potential physiological significance of high-frequency BOLD signal (Chen and
94 Glover 2015) is under debate. To measure the effects of neural activity in different
95 frequency bands, the frequency range was generally subdivided into four sub-
96 frequency bands, including slow-5 (0.01 - 0.027 Hz), slow-4 (0.027 - 0.073 Hz), slow-
97 3 (0.073 - 0.198 Hz) and slow-2 (0.198 - 0.25 Hz) based on previous
98 electrophysiological (Buzsaki and Draguhn 2004) and fMRI studies (Zuo et al. 2010).
99 Inhomogeneous spatial amplitude of low-frequency fluctuations (ALFF) distribution
100 between slow-4 and slow-5 were observed (Zuo et al. 2010). Furthermore, frequency-
101 specific ALFF changes have been found in disease groups such as mild cognitive
102 impairment (Han et al. 2011), Parkinson’s disease (Hou et al. 2014) and depression
103 (Wang, Kong, et al. 2016) between slow-4 and slow-5. Besides, frequency-specific
104 effects have also been widely reported in functional connectivity (Gohel and Biswal
105 2015), regional homogeneity (ReHo) (Yu et al. 2016), and brain networks (Xue et al.
106 2014). These findings indicate the underlying frequency-dependent brain activity and
107 frequency-specific disease alterations. While for CAPs, whether and how would the
108 spatial and temporal characteristics change with the frequency band is unknown and
109 remains to be explored.

110 Schizophrenia is a mental disorder with globally altered brain functions, and the
111 aberrant brain dynamics found in schizophrenia patients (SZ) have the potential to be
112 the biomarker to reveal the complex pathology of this disease (Du et al. 2017;
113 Kottaram et al. 2018). The abnormal dynamic brain graphs (Yu et al. 2015) and
114 network reconfigurations have also been identified in SZ (Reinen et al. 2018). Our

115 previous study has shown the altered CAP state dynamics of SZ patients were not
116 only involved with the triple-network, but also extend to other primary and high-order
117 networks (Yang et al. 2021). Besides the dynamic brain changes, SZ patients also
118 showed frequency-specific alterations in several aspects, including ALFF (Yu et al.
119 2014; Gohel et al. 2018; Meda et al. 2015; Hare et al. 2017), ReHo (Yu et al. 2013),
120 BOLD variability (Zhang, Yang, and Cai 2020), as well as functional connectivity
121 (Wang et al. 2017; Han et al. 2017). Furthermore, Zou and colleagues distinguished
122 schizophrenia patients from healthy controls using the dFC estimated at different
123 frequency bands (Zou and Yang 2019), and Luo et al. found that SZ showed distinct
124 dFC strength alterations in slow-4 and slow-5 (Luo, He, et al. 2020), these results
125 suggest the underlying frequency-specific dynamic alterations in psychosis. Based on
126 the above findings, SZ patients may also be affected by frequency-specific CAP
127 alterations that need further investigations.

128 The purpose of this study is to test whether the frequency-dependent effects can
129 be observed using coactivation patterns. Specifically, the typical range (0.01 – 0.08
130 Hz) and four sub-frequency bands from slow-5 to slow-2 were analyzed, and CAP
131 analysis was performed in each frequency band separately. Then, the spatial and
132 temporal characteristics varied with frequency bands were evaluated, and particularly
133 the results of slow-4 and slow-5 were statistically compared, as these two sub-
134 frequency bands are within the typical low-frequency range and have been widely
135 studied in previous studies. Finally, the frequency-dependent CAPs were applied to
136 schizophrenia patients, and the frequency-specific disease alterations were studied in
137 this work.

138

139 **2. Materials and methods**

140 **2.1 Participants**

141 All participants were scanned at the Department of Medical Imaging, Wuxi
142 People's Hospital, Nanjing Medical University. Four subjects were excluded due to
143 the large headmotion. As shown in Table 1, 69 schizophrenia patients (35 males/34

144 females, 46.06 ± 10.96 years) and 97 healthy controls (56 males/41 females, $40.36 \pm$
145 14.77 years) remained for the current study. Positive and Negative Syndrome Scale
146 (PANSS) was performed for all schizophrenia patients to evaluate their symptom
147 severity. This research was approved by the Medical Ethics Committee of Wuxi
148 Mental Health Center, Nanjing Medical University (study number:
149 WXMHCIRB2012LLKY001), and was conducted in accordance with the Declaration
150 of Helsinki guidelines. The written informed consent was obtained from all
151 participants.

152

153 **Table 1.** The demographic information for the WuXi cohort

WuXi	All - HC (n = 97)	Matched - HC (n = 69)	SZ (n = 69)	P value
Age	40.36 ± 14.77	45.84 ± 11.89	46.06 ± 10.96	0.9112 ^{a)}
Gender (M \ F)	56 \ 41	35 \ 34	35 \ 34	1 ^{b)}
Disease duration	-	-	19.84 ± 10.96	-
PANSS positive	-	-	20.06 ± 4.59	-
PANSS negative	-	-	23.78 ± 3.84	-
PANSS general	-	-	41.67 ± 5.27	-
PANSS total	-	-	85.51 ± 9.50	-

154 Data are expressed as mean \pm SD (SD: standard deviation).

155 Abbreviations: PANSS, Positive and Negative Syndrome Scale.

156 ^{a)} two-sample t-test; ^{b)} chi-square cross-table test.

157

158 2.2 fMRI Data Acquisition

159 Three-dimensional T1-weighted images and resting-state fMRI scans were
160 collected using a 3.0 T Magnetom TIM Trio (Siemens Medical System). Structural
161 MRI images were acquired using a 3D-MPRAGE sequence with the following
162 parameters: TR/TE = 2530/3.44 ms, flip angle = 7° , FOV = 256 mm, matrix
163 size = 256×256 , voxel size = $1 \times 1 \times 1$ mm³, slice thickness = 1 mm and slice number
164 = 192. Resting-state fMRI data were obtained using a single-shot gradient-echo echo-
165 planar-imaging sequence, with TR/TE = 2000/30 ms, flip angle = 90° , FOV = 220 mm,
166 matrix size = 64×64 , voxel size = $3.4 \times 3.4 \times 4$ mm³, slice thickness = 4 mm, slice
167 number = 33, and 240 volumes were collected for each subject.

168

169 **2.3 Data Preprocessing**

170 All structural and functional MRI images were preprocessed using DPABI
171 (<http://rfmri.org/dpabi>). The T1-weighted images were first coregistered to the
172 functional images, and then segmented into gray matter, white matter and
173 cerebrospinal fluid by using DARTEL. For the resting-state fMRI images, the first 5
174 time points were removed to avoid instability of the scanner, and the remaining
175 images were realigned to correct the head movement. Framewise displacement (FD)
176 was calculated for each subject (Di and Biswal 2015), and subjects with maximum
177 translation or rotation FD greater than 2 mm or 2° were excluded from further
178 analysis. The fMRI images were normalized to the Montreal Neurologic Institute
179 (MNI) space using the deformation field maps obtained from the T1 segmentation,
180 and resampled to $3 \times 3 \times 3$ mm³. The mean white matter, cerebrospinal fluid and
181 global signal, and 24 head motion parameters (Friston et al. 1996) were regressed
182 from the time series. The time series was further detrended and temporal filtered.
183 Besides the typical filtering bandpass (0.01 - 0.08 Hz), another four sub-bands
184 including slow-5 (0.01 - 0.027 Hz), slow-4 (0.027 - 0.073 Hz), slow-3 (0.073 - 0.198
185 Hz) and slow-2 (0.198 - 0.25 Hz) were employed separately based on the previous
186 study (Zuo et al. 2010). Finally, all images were smoothed using an 8 mm FWHM
187 Gaussian kernel.

188 Similar to our previous study, the mean BOLD time series was extracted from
189 408 ROIs separately (Yang et al. 2021), which includes 400 cortical regions (Schaefer
190 et al. 2018) and 8 subcortical regions (bilateral caudate nucleus, putamen, globus
191 pallidus and amygdala) from the AAL template (Tzourio-Mazoyer et al. 2002). The
192 400 cortical regions belong to 7 networks, including the visual network (VN),
193 somatomotor network (SMN), dorsal attention network (DAN), ventral attention
194 network (VAN), limbic network, fronto-parietal network (FPN) and default mode
195 network (DMN).

196

197 **2.4 Coactivation Pattern Analysis**

198 The coactivation pattern (CAP) analysis is a data-driven method based on the k-
199 means clustering, and it is supposed to identify recurring whole-brain coactivation
200 states. The same analysis pipeline from our previous work (Yang et al. 2021) was
201 used to detect the CAP states in different frequency bands.

202 In brief, there were 235 volumes for each subject, and each volume was
203 characterized by the activation level of 408 ROIs. The time series of each ROI was
204 first normalized using z-score independently, and the absolute value of Z indicates the
205 activation deviation from its baseline. Then, K-means clustering was performed based
206 on all volumes from the 97 HC subjects, and volumes sharing similar coactivation
207 profiles were grouped into the same CAP state. The spatial map of each CAP was
208 obtained by averaging across volumes belonging to the state, and divided by their
209 standard deviation to generate a Z-map (Liu and Duyn 2013). Pearson correlation was
210 used to measure the spatial similarity between volumes and CAP states. As for the SZ
211 subjects, their volumes were assigned to the obtained CAP state with the highest
212 spatial similarity. The cluster number K was tested from 2 to 21, and the silhouette
213 score (Rousseeuw 1987) was used to determine the cluster number. Our previous
214 work identified six robust CAP states in the typical range (H. Yang et al., 2021). We
215 found six clusters were also suitable for the four sub-frequency bands, and their
216 silhouette score curves were shown in Supplementary Figure S1.

217

218 **2.5 CAP state temporal dynamic measures**

219 The temporal dynamic properties among the six CAP states were evaluated using
220 four CAP metrics at the individual level. **Fraction of time** represents the proportion
221 of time occupied by one state. **Persistence** describes the average dwell time, and
222 **Counts** records the frequency of one state that occurs across the scan. In addition to
223 these state dominances that capture the inner-state dynamics, the **transition**
224 **probability** between states was also measured and presented in the supplementary
225 materials.

226

227 **2.6 Statistical Analysis**

228 For comparisons within the HC group, all 97 HC subjects were analyzed, and for
229 comparisons between SZ and HC, only age- and gender-matched HC subjects were
230 included (69 HC and 69 SZ). For the demographic data, two-sample t-test was used to
231 compare the age difference between SZ and HC, and chi-square cross-table test was
232 used to test their gender difference.

233 In this study, the spatial and temporal characteristics of CAPs in slow-5 (0.01 -
234 0.027 Hz) and slow-4 (0.027 - 0.073 Hz) were further compared, as they constitute
235 most power of the typical low-frequency range (0.01 – 0.08 Hz). For the CAP results
236 within the HC group, the six CAPs of slow-5 and slow-4 were compared at the ROI
237 level using paired t-test, and Bonferroni correction was used to correct the multiple
238 comparisons ($p < 0.05/408$) for each state. To better illustrate the 408 ROIs' group
239 averaged activation level in slow-4 and slow-5 (the first two columns in Figure 4),
240 boxplots were plotted for the six CAPs, and the 408 ROIs were categorized into the
241 seven networks. As for the temporal dynamic measures, the CAP matrices were
242 compared between slow-5 and slow-4 using paired t-test, and p values were false-
243 discovery rate (FDR) adjusted. Besides, the between-state temporal differences were
244 also examined using paired t-test in slow-4 and slow-5 separately, and Bonferroni
245 correction was performed.

246 Furthermore, the CAP dynamic differences between SZ and HC in slow-5 and
247 slow-4 were studied, and the group \times frequency interaction effects were estimated
248 using a two-way repeated-measures analysis of variance (ANOVA) with age and
249 gender as covariates, and FDR correction was performed to account for the multiple
250 comparisons. For post hoc comparisons, two-sample t-test (with age and gender
251 controlled) was performed to clarify the group differences, and paired t-test was used
252 to detect the frequency effects. FDR correction was performed across all post hoc
253 tests.

254

255 **2.7 Classification Analysis**

256 To further investigate that whether combining slow-5 and slow-4 contains more
257 information and improves the classification accuracy of schizophrenia patients than
258 just using the typical range, eight classification models have been built using temporal
259 or spatial features from typical range, slow-5, slow-4 separately, and combined slow-5
260 and slow-4. In this study, we used a similar classification model and feature selection
261 strategy with our previous work (Yang et al. 2020), and the details were illustrated in
262 the supplementary materials.

263

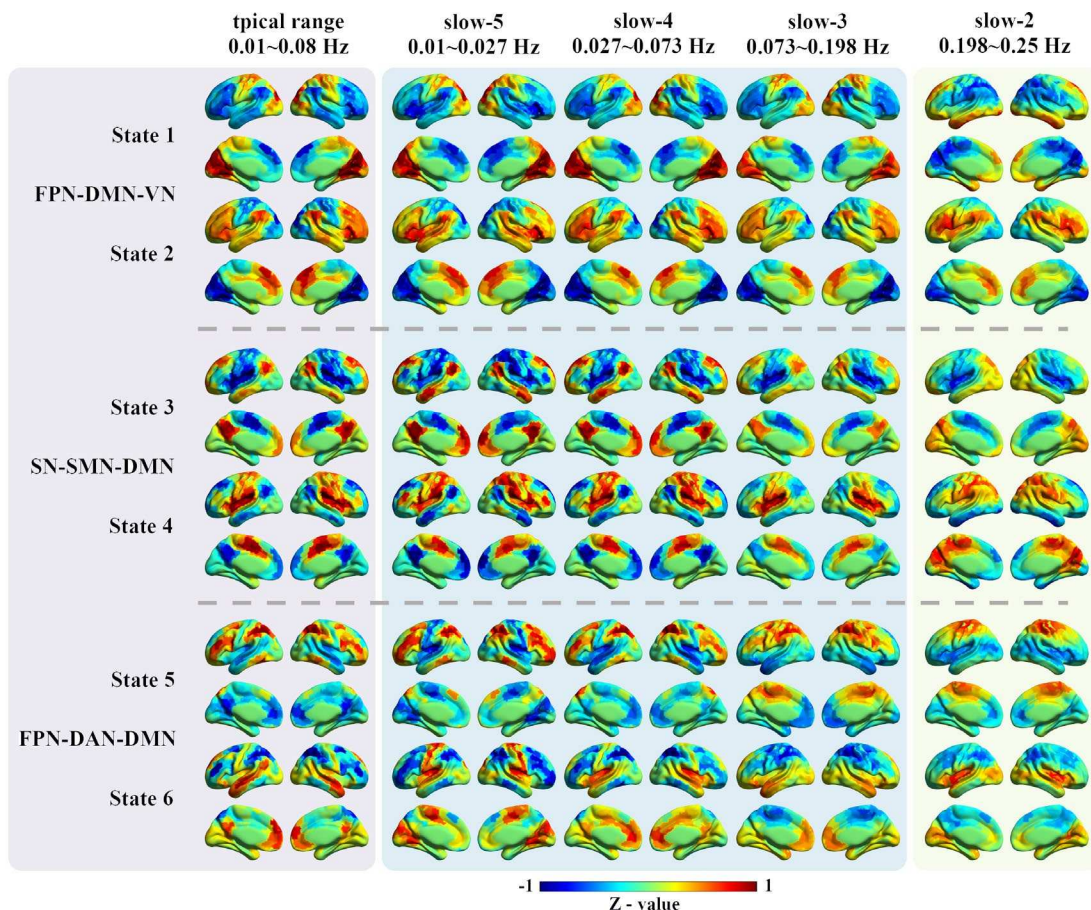
264 **3. Results**

265 **3.1 Spatial and temporal properties of CAPs at different frequency bands**

266 The CAP analysis was performed in all 97 HC subjects in the typical range and
267 four sub-frequency bands (slow-5 to slow-2) separately. As shown in Figure 1, typical
268 intrinsic high-order (e.g., FPN and DMN) and primary networks (e.g., VN and SMN)
269 can be observed in the typical range, slow-5, slow-4 and slow-3. While some of them,
270 particularly the high-order networks disappeared in slow-2, for instance, the DMN
271 and FPN cannot be found in any state in slow-2. Pearson correlation was calculated
272 between each pair of states to quantify the CAPs spatial similarities between the
273 typical range and the other four frequency bands (Figure 2). All six CAP states
274 showed high spatial one-to-one correspondence between slow-4 and the typical range,
275 as can be observed from the diagonal of the matrix (Figure 2B), followed by slow-5
276 and slow-3. As for slow-2, only State 2 and State 3 were similar to the typical range.

277 The absolute value of activation amplitude of each ROI indicates the deviation
278 from its baseline activation level (Z value = 0), and was defined as activation
279 deviation in this work. A larger activation deviation means a stronger positive
280 activation or stronger negative deactivation. For example, compared with other brain
281 areas, regions within the visual network exhibited stronger positive activation in State
282 1, and stronger negative deactivation in State 2. Hence, we said that State 1 and State
283 2 showed larger activation deviation in the visual network, and the visual network was
284 the dominant network for State 1 and State 2.

285 In our previous study, the six CAP states were grouped into three pairs (State 1
 286 and State 2, State 3 and State 4, State 5 and State 6) in the typical range, and the
 287 paired CAP states were characterized by opposite coactivation profiles. In the typical
 288 range, State 1 and State 2 were mainly dominated by VN, FPN and DMN, State 3 and
 289 State 4 were mainly dominated by SN, SMN and DMN, and State 5 and State 6 were
 290 mainly dominated by FPN, DAN and DMN. The between-state spatial similarity
 291 matrix was measured for each sub-frequency band independently in this study, and
 292 the spatially opposite CAP pairs can also be observed in the four sub-frequency bands
 293 (supplementary Figure S2). For instance, State 3 and State 4 belong to an opposite
 294 CAP-pair. The DMN was activated, and the SMN and SN were deactivated in State 3,
 295 while the DMN was deactivated, and the SMN and SN were activated in State 4.
 296

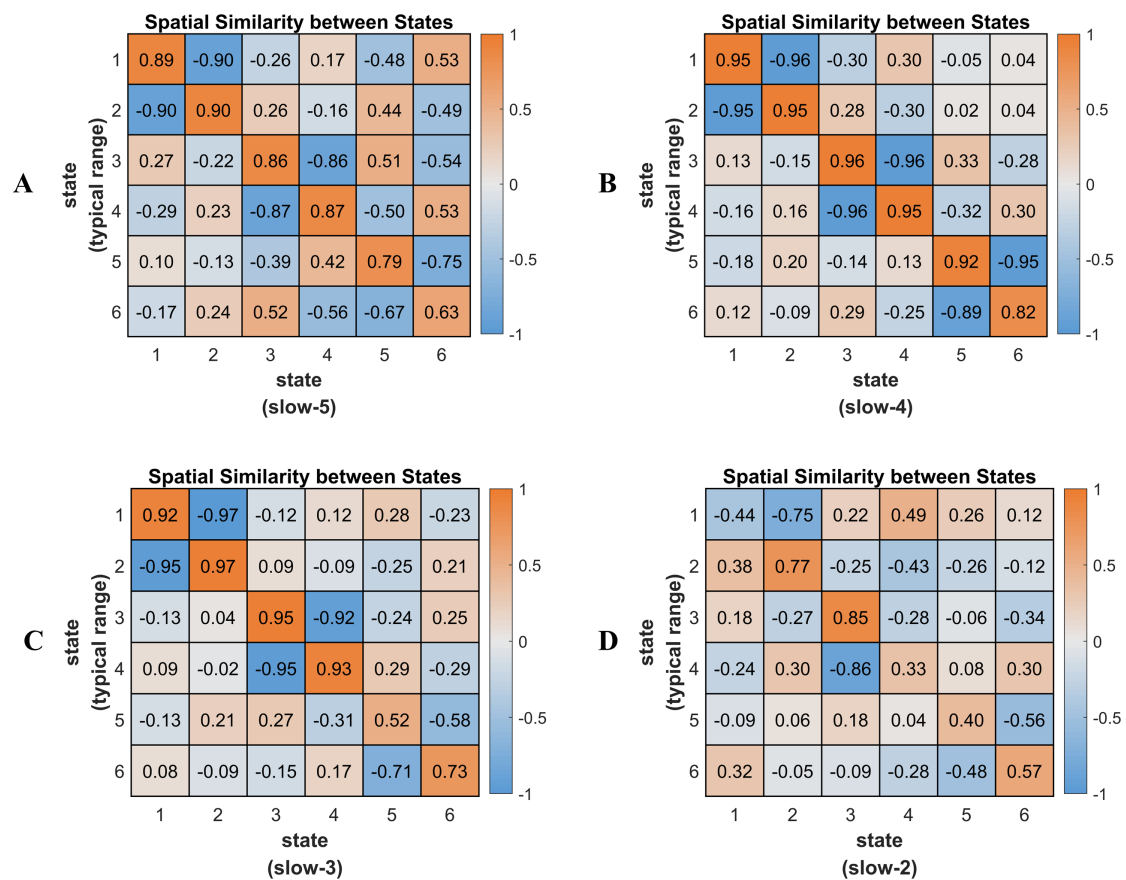


297
 298 **Figure 1.** The spatial patterns for the six CAP states in different frequency bands. The
 299 first column shows the six CAP states in the typical range, and the six states were
 300 grouped into three pairs with opposite coactivation profiles. The following four

301 columns show the six CAP states from slow-5 to slow-2. For each ROI, the Z-value
 302 means the degree of activation deviation from its baseline. The warm color indicates a
 303 relatively stronger BOLD response than its baseline amplitude, and vice versa for the
 304 cold color.

305 Abbreviations: DAN, dorsal attention network; DMN, default mode network; FPN,
 306 fronto-parietal network; SN, salience network; SMN, somatomotor network.

307



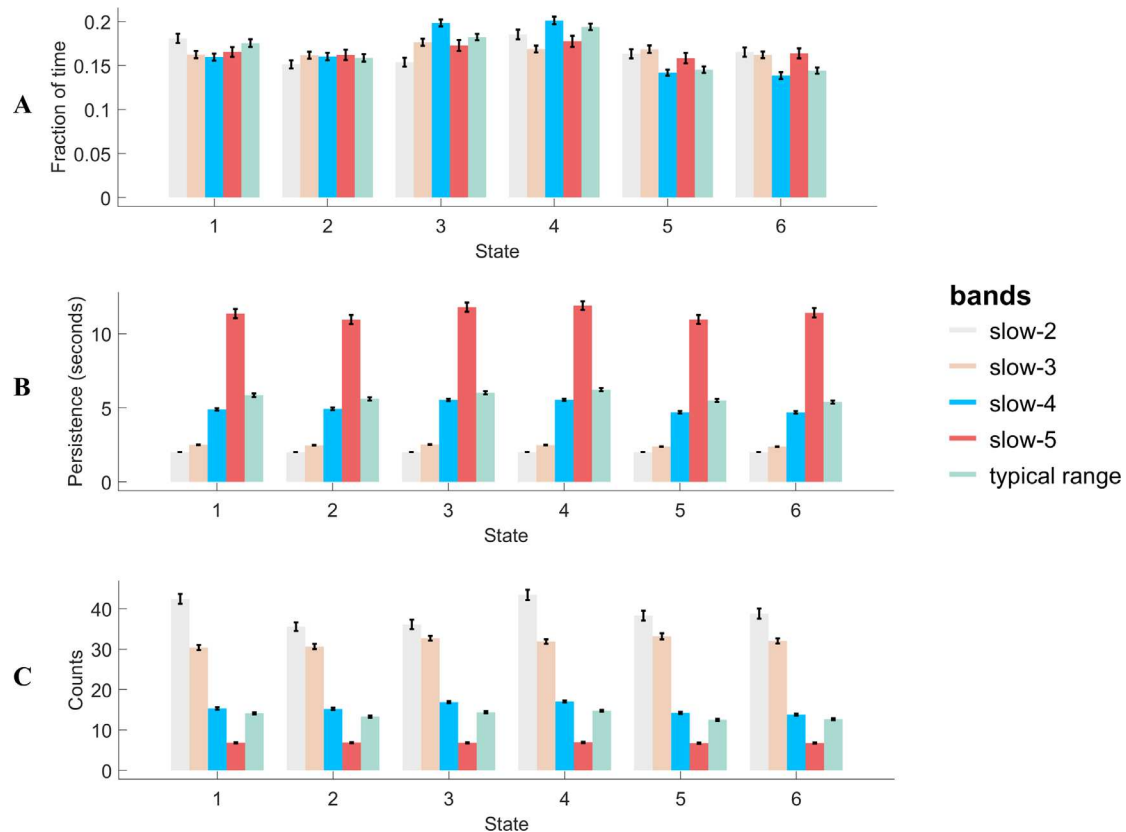
308

309 **Figure 2.** The CAP spatial similarity between the typical range and four sub-
 310 frequency bands. Pearson correlation was calculated to measure their spatial
 311 similarity, and the colorbar shows the R-value.

312

313 The temporal dynamics in the typical range and four sub-frequency bands were
 314 then compared and shown in Figure 3. The mean fraction of time was comparable
 315 across the six CAP states for all frequency bands, around 15% to 20%. As for the
 316 persistence, with the decrease of frequency bands from slow-2 to slow-5, each state

317 persisted longer before it transfers to another state. For slow-2 and slow-3, each state
318 would only persist for about 2 seconds, and increased to about 5 seconds for slow-4
319 and 12 seconds for slow-5. The persistence of the typical range was between slow-4
320 and slow-5, which was around 6 seconds. On the contrary, counts (occurrences of
321 state) decreased with the decrease of the frequency band.
322



323
324 **Figure 3.** The state temporal dominances (fraction of time, persistence and counts) in
325 the typical range and four sub-frequency bands. The error bar shows the standard
326 error.

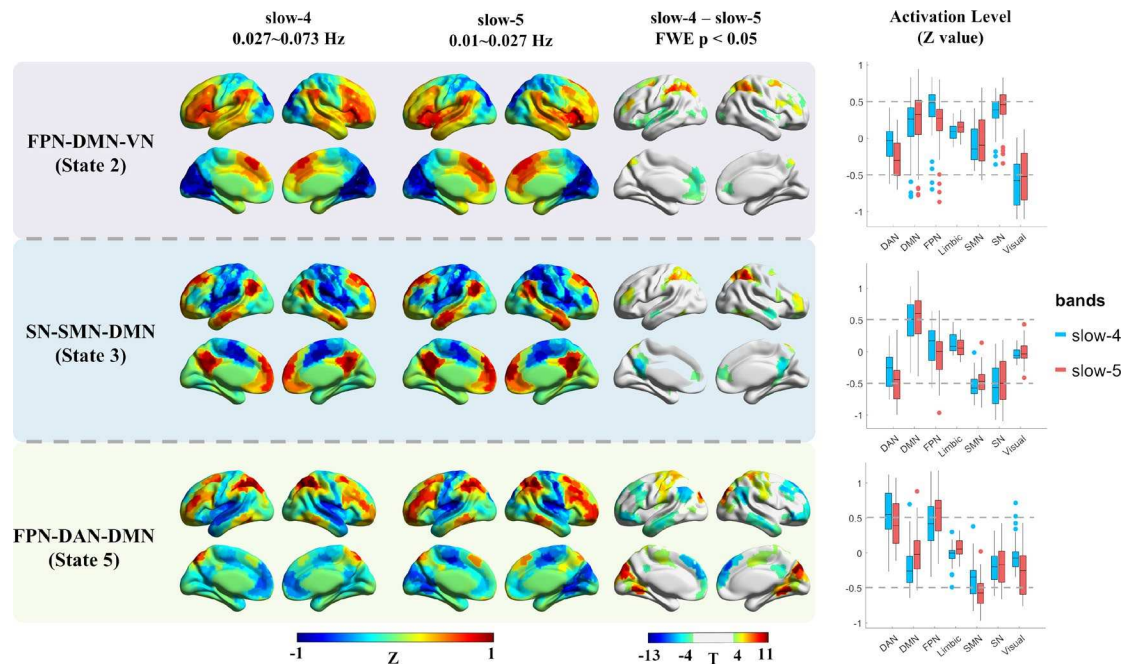
327

328 3.2 Specific spatial and temporal characteristics of CAPs in slow-4 and slow-5

329 To further investigate that, within the typical low-frequency range (0.01 - 0.08
330 Hz), whether the two popular studied sub-frequency bands (slow-4 and slow-5)
331 showed frequency-specific spatial and temporal characteristics, the spatial maps and
332 CAP dynamics were statistically compared within the HC group. As described in the
333 supplementary Figure S5, for the six CAP states between slow-4 and slow-5, one-to-

334 one correspondence can be established based on CAPs' spatial similarity. As the six
335 states were grouped into three pairs with opposite coactivation patterns (State 1 and 2,
336 State 3 and 4, State 5 and 6), similar regions showed frequency-specific activation
337 differences for the paired states, hence we only showed half of the results (Figure 4),
338 and the remained results were described in the supplementary Figure S6. To make the
339 naming rule consistent with our previous results based on the typical range (Figure 1),
340 the three states were still named as FPN-DMN-VN, SN-SMN-DMN and FPN-DAN-
341 DMN. The group averaged activation levels of the seven networks in slow-4 and
342 slow-5 were also shown in the last column of Figure 4.

343 It can be observed that, State 1 and 2 were characterized by large activation
344 deviation in the VN in both slow-4 and slow-5, then followed by SN and FPN.
345 Compared with slow-5, slow-4 showed larger activation deviation in the bilateral
346 middle frontal gyrus (FPN), and less activation deviation in the bilateral insula (SN)
347 and dorsal attention network (DAN) in both State 1 and 2. Slow-4 also exhibited less
348 anterior DMN activation in State 2. As for State 3 and 4, they were dominated by the
349 SN, SMN and DMN in both slow-4 and slow-5, and slow-4 showed less activation
350 deviation in the DMN and FPN. Besides, slow-5 was also dominated by the DAN,
351 hence stronger activation deviation in the DAN was observed in slow-5. Finally, State
352 5 and 6 showed large DAN and FPN activation deviation in both slow-4 and slow-5,
353 while slow-5 was also dominated by the SMN. In general, slow-5 showed an overall
354 stronger activation deviation in the SMN, FPN and VN, and slow-4 showed a stronger
355 activation deviation in the DMN.



356

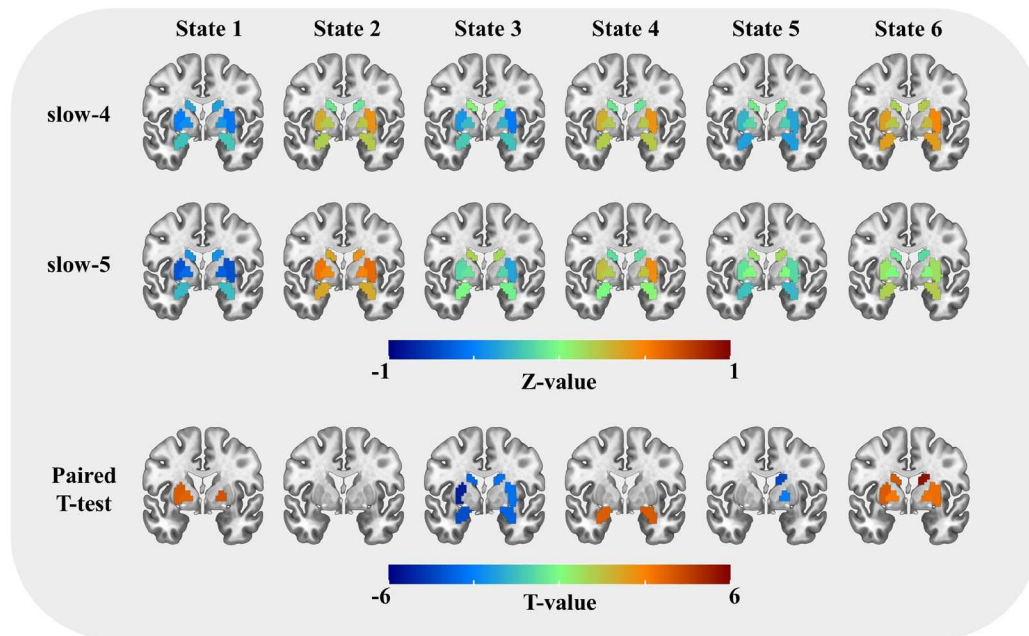
357 **Figure 4.** The frequency-specific effects between slow-4 and slow-5 within the HC
 358 group. The results of three states were presented, as the six CAP states were grouped
 359 into three pairs, and similar results were found within the pair. The first two columns
 360 show the cortical coactivations, and the color of each ROI indicates the activation
 361 deviation from its baseline level (Z-value). Paired t-test was performed for each state
 362 separately, and Bonferroni correction was used at the ROI level. The colorbar shows
 363 the T-value, and regions with $P < 0.05$ (FWE corrected) were presented in the third
 364 column. The last column shows the activation level of the seven networks in slow-4
 365 and slow-5, and each point represents an ROI's group averaged activation level from
 366 all 97 HC subjects.

367 Abbreviations: DAN, dorsal attention network; DMN, default mode network; FPN,
 368 fronto-parietal network; SN, salience network; SMN, somatomotor network.

369

370 In addition, frequency-specific activation differences have also been found in
 371 several subcortical regions after FDR correction ($p < 0.005$, FDR adjusted). Slow-4
 372 exhibited an overall stronger subcortical activation deviation than slow-5 (Figure 5).
 373 Particularly, slow-4 showed stronger activations at the bilateral basal ganglia (caudate
 374 nucleus, putamen and globus pallidus) in State 6, stronger deactivations at the right
 375 caudate nucleus and globus pallidus in State 5, stronger activations at the bilateral

376 amygdala in State 4, and stronger deactivations at the bilateral caudate nucleus,
377 putamen and amygdala in State 3. Nevertheless, weaker deactivations at bilateral
378 globus pallidus and left putamen were also found in slow-4 in State 1.
379



380
381 **Figure 5.** The subcortical activation differences between slow-4 and slow-5 within
382 the HC group. The first two rows show the coactivations of the eight subcortical
383 regions, and the color of each ROI indicates the activation deviation from its baseline
384 level (Z-value). Paired t-test was performed for six states separately, and FDR
385 correction was used at the ROI level. Regions with $P < 0.005$ (FDR adjusted) were
386 presented in the last row, and the colorbar shows the T-value.

387
388 Next, the CAP temporal dynamics in slow-4 and slow-5 within the HC group
389 were quantitatively compared using a paired t-test (supplementary Figure S7A).
390 Compared with slow-5, all six states showed significantly shorter persistence and
391 more counts in slow-4. More fraction of time in State 3 and State 4, and less fraction
392 of time in State 5 and State 6 were observed in slow-4. In addition, the variation of
393 fraction of time between the six states was also evaluated in slow-4 and slow-5
394 separately (supplementary Figure S7B). No between-state difference was found in

395 slow-5, that each state occupied about 15% - 17% of the time. However, significant
396 between-state differences were found in slow-4, e.g., State 3 and 4 showed more
397 fraction of time (about 20 %) than the other four states, and State 6 accounted for the
398 least amount of time.

399

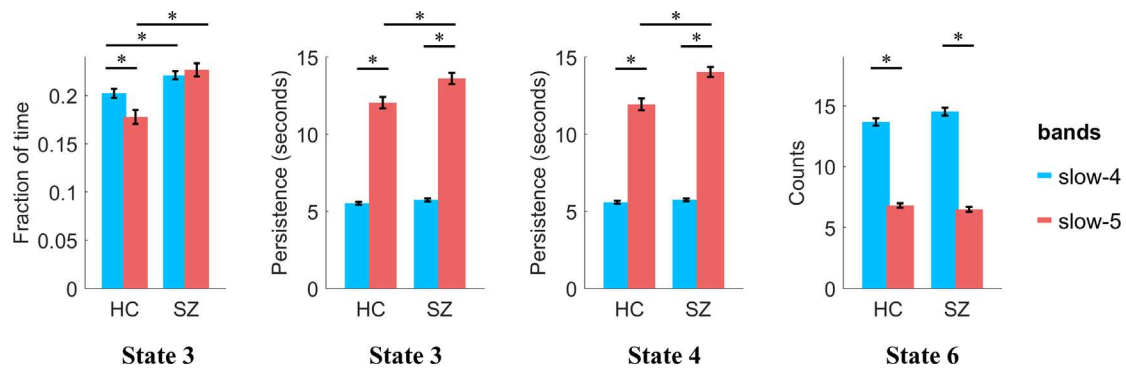
400 **3.3 Frequency-specific CAP dynamic alterations in SZ**

401 The CAP differences between SZ and HC have been examined in the typical
402 range before (Yang et al. 2021), then the frequency-specific alterations in slow-4 and
403 slow-5 were further studied in this work. Two-way repeated-measures ANOVA was
404 performed to estimate the main effects and interaction effects between group and
405 frequency.

406 Significant group main effects were found in several states. SZ showed decreased
407 fraction of time in State 1 and State 2, and increased fraction of time in State 3 and
408 State 4. SZ also showed decreased persistence in State 2 and State 6, and increased
409 persistence in State 3 and State 4. Finally, decreased counts in State 1 and State 2, and
410 increased counts in State 3 and State 4 were observed in SZ. Significant frequency
411 main effects on fraction of time were also found. Fraction of time increased in State 3
412 and State 4 and decreased in State 5 in slow-4. For persistence and counts, significant
413 frequency main effects were obtained in all six states. As described before, higher-
414 frequency (slow-4) CAPs showed shorter persistence and more counts than lower-
415 frequency (slow-5). The detailed statistic results were presented in Supplementary
416 Table S4.

417 Significant frequency-group interaction effects were found on fraction of time (P
418 = 0.0014, $F = 11.0473$) in State 3, persistence in State 3 ($P = 0.0084$, $F = 7.38$) and
419 State 4 ($P = 4.48 \times 10^{-4}$, $F = 13.61$), and counts in State 6 ($P = 0.0465$, $F = 4.11$). For
420 post hoc results, we mainly reported the group differences. SZ showed increased
421 fraction of time in State 3 in both slow-4 ($P = 0.0058$, $T = 2.93$) and slow-5 ($P = 6.23$
422 $\times 10^{-6}$, $T = 4.90$) than HC. Besides, SZ also showed increased persistence in both

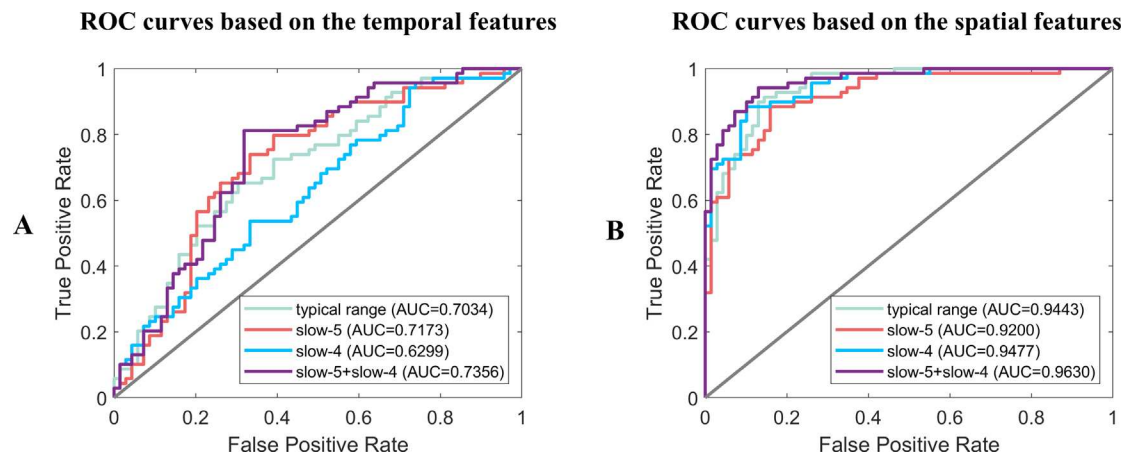
423 State 3 ($P = 0.0052$, $T = 3.00$) and State 4 ($P = 1.04 \times 10^{-4}$, $T = 4.18$) in slow-5 than
424 HC. No group difference was obtained in either slow-4 or slow-5 on counts.
425



426 **Figure 6.** The post hoc results of repeated two-way ANOVA, only the results with
427 significant interaction effects were compared. Between-group differences were
428 compared using two-sample t-test, and between-frequency differences were compared
429 using paired t-test. Age and gender were controlled for between-group comparisons,
430 and FDR correction was performed to correct the multiple comparisons. Error-bar
431 shows the standard error. * indicates $p < 0.05$ with FDR correction.
432

433
434 As for the classification results, the ROC (receiver operating characteristic)
435 curves and their AUC (Area Under Curve) values were shown in Figure 7. Generally,
436 the spatial features resulted in a higher classification accuracy than the temporal
437 features, and combining slow-5 and slow-4 would increase the AUC than only using
438 the typical range. The best classification results were obtained by combining the
439 spatial features from both slow-5 and slow-4, with $AUC = 0.9630$, $Accuracy =$
440 0.8913 , $Sensitivity = 0.8986$ and $Specificity = 0.8841$. The detailed results can be
441 found in Supplementary Table S5 and Table S6.

442



443

444 **Figure 7.** The ROC curves and AUC values of classification results based on the (A)
445 temporal features and (B) spatial features in the typical range, slow-5, slow-4
446 separately and combined slow-5 with slow-4.

447

448 **4. Discussion**

449 This work systematically investigated the frequency-specific coactivation patterns
450 across slow-2 to slow-5 and compared their spatial and temporal characteristics with
451 the results obtained from the typical range. Particularly, slow-4 and slow-5 were
452 further compared within healthy subjects, and the frequency-specific CAP dynamic
453 alterations in schizophrenia patients were studied. Generally, both the high-order and
454 primary networks can be observed across slow-5 to slow-3 except slow-2, and the
455 CAP state persisted shorter and occurred more frequently at a higher frequency band.
456 In addition, stronger subcortical coactivations and co-deactivations were observed in
457 slow-4, while large-scale function networks such as DAN showed stronger
458 coactivations and co-deactivations in slow-5. Furthermore, schizophrenia patients
459 showed frequency-specific alterations in slow-4 and slow-5, and combining slow-4
460 and slow-5 increased the classification accuracy.

461

462 **4.1 Spatial and temporal properties of CAPs at different frequency bands**

463 The coactivation patterns in the typical range (0.01 - 0.08 Hz) have been
464 demonstrated in our previous study (Yang et al. 2021), and the four sub-frequency
465 bands were further studied in this study. Compared with the typical range, slow-5

466 (0.01 - 0.027 Hz), slow-4 (0.027 - 0.073 Hz) and slow-3 (0.073 - 0.198 Hz) showed
467 similar spatial patterns, which were characterized by typical functional networks.
468 Consistent with previous studies (Huang et al. 2020; Zhang et al. 2020), opposite CAP
469 pairs were also found in the sub-frequency band, suggesting the antagonistic
470 relationships between these intrinsic networks widely exist at different sub-frequency
471 bands. However, the CAP states in slow-2 (0.198 - 0.25 Hz) were unlike that of the
472 typical range, brain regions belonging to the same network were not coactivated
473 together or mixed with other networks. A previous study has found that slow-2 mainly
474 oscillates within white matter rather than grey matter (Zuo et al. 2010). Gohel and
475 Biswal (Gohel and Biswal 2015) evaluated the seed-based correlation maps from
476 slow-5 to slow-1, and they found the spatial extent of slow-2 was significantly
477 reduced compared with slow-5/4/3. Together, these findings indicate the attenuated
478 intrinsic functional associations in slow-2. The reason might be that the resting-state
479 brain and intrinsic functional networks were mainly activated at the low-frequency,
480 and there were also more physiological noises at the higher frequency (Cordes et al.
481 2001; Chen and Glover 2015).

482 As for the CAP dynamics, persistence and counts changed monotonically with
483 the increased frequency band. Particularly, persistence decreased, and counts
484 increased for all the six states from slow-5 to slow-2, suggesting that the higher
485 frequency led to unstable state maintenance. First, the higher frequency could cause
486 more frequent BOLD fluctuations, hence the volume-to-volume state maintenance
487 would decrease, and the between-state transition would increase. As the fraction of
488 time was similar across different frequency bands, shorter persistence would lead to
489 more counts. Besides, the higher frequency BOLD signal involved more noises
490 (Cordes et al. 2001; Chen and Glover 2015), which might affect the coactivation
491 profile and result in more between-state transitions, and shorten the persistence.

492

493 **4.2 Specific spatial and temporal configurations of CAPs in slow-4 and slow-5**

494 Previous studies have found that the neural oscillations of the human brain are
495 frequency-dependent. Particularly, large-scale functional networks (e.g., DMN and
496 FPN) integrate remote brain regions with long-distance interactions (Salvador et al.
497 2005), and these functional processes are primarily achieved by a lower-frequency
498 band (Buzsaki and Draguhn 2004; Penttonen, Buzsáki, and Systems 2003). On the
499 contrary, subcortical regions are spatially compact and dominated by local neural
500 activities (Salvador et al. 2005), and these short-range connections work in a higher-
501 frequency band (Buzsaki and Draguhn 2004).

502 In our results, generally the whole-brain spatial patterns of the six CAP states in
503 slow-4 and slow-5 were similar to the typical range, which were characterized by the
504 coactivation or co-deactivation of large-scale intrinsic networks, while frequency-
505 specific coactivation profiles were still found between slow-4 and slow-5. Stronger
506 DAN, DMN and FPN activation deviations were observed in slow-5 in several CAP-
507 states. Especially, DAN showed larger activation deviation in slow-5 across State 1 to
508 State 4, suggesting the activity of DAN mainly fluctuates at the lower frequency band.
509 Slow-5 showed stronger DMN activation deviation in State 3 and 4, and stronger
510 anterior DMN activation in State 2. Previous studies have also found greater
511 ALFF/fALFF in several DMN regions in slow-5 (Han et al. 2011; Wang, Kong, et al.
512 2016). Subcortical regions showed larger activation deviations in slow-4 for most
513 CAP states, for instance, slow-4 showed stronger activation at bilateral basal ganglia
514 in State 6, which was consistent with previous findings that stronger basal ganglia
515 ALFF/fALFF in slow-4 (Zuo et al. 2010). The above results support the previous
516 findings that large-scale functional networks are mainly mediated by lower-frequency
517 connections, while higher-frequency activities are linked with subcortical systems
518 (Buzsaki and Draguhn 2004; Han et al. 2011; Wang, Kong, et al. 2016).

519 However, different compared with previous results, stronger FPN activation
520 deviation has been observed in slow-4 in State 1 and 2, and stronger DMN activation
521 deviation has been found in slow-4 in State 5 and 6. Furthermore, a few subcortical
522 regions (globus pallidus and putamen) also showed weaker activation deviations in

523 slow-4 in State 1. It is worth noting that, previous conclusions were mainly drawn
524 from static studies, while the frequency-specific properties might change dynamically,
525 and the subcortical-related high-frequency band (0.3032–0.4545 Hz) studied before is
526 (Salvador et al. 2005) even higher than slow-2 (0.198 - 0.25 Hz). While both slow-5
527 (0.01 - 0.027 Hz) and slow-4 (0.027 - 0.073 Hz) still belong to the typical low-
528 frequency range (0.01 - 0.08 Hz), which might be the reason why the subcortical and
529 large-scale networks were not always stronger in slow-4 or slow-4 across all states.
530 Therefore, these results suggest that within the typical low-frequency range, although
531 both slow-4 and slow-5 showed similar coactivation patterns, the large-scale networks
532 and subcortical regions might still be mediated by different frequency bands at
533 specific periods and brain states.

534 As for the temporal domain, slow-4 showed significantly shorter persistence and
535 more counts across all the six CAPs. Due to the long persistence and high within-state
536 transition probability, fewer between-state transitions occurred in slow-5, suggesting
537 the integration of large-scale networks requires sufficient time to maintain a relatively
538 stable state and execute specific functions based on the lower-frequency signals.
539 Besides, an unbalanced between-state fraction of time was found in slow-4 but not in
540 slow-5 (Figure S7B). State 3 and 4 showed more fraction of time than the other four
541 CAPs in slow-4, and State 5 and 6 showed the least fraction of time. Hence, slow-4
542 showed a significantly increased fraction of time in State 3 and 4, and decreased
543 fraction of time in State 5 and 6. The unbalanced between-state time allocation and
544 more frequent between-state transitions together suggest the richer temporal dynamics
545 in slow-4.

546

547 **4.3 Frequency-specific CAP differences between SZ and HC in slow-4 and slow-5**

548 Previous studies have shown that SZ patients are not only characterized by
549 frequency-specific changes (Gohel et al. 2018; Yu et al. 2013; Zhang, Yang, and Cai
550 2020) or temporal dynamic changes (Du et al. 2017; Kottaram et al. 2018), but also
551 frequency-specific dynamic alterations (Zou and Yang 2019; Luo, He, et al. 2020).

552 Our previous study has demonstrated the altered CAP dynamics between SZ and HC
553 in the typical range (Yang et al. 2021), and the frequency-specific alterations in SZ
554 were further studied in the current work. In general, a similar trend of case-control
555 differences across the six states was observed at both slow-4, slow-5 and the typical
556 range. Consistent with the typical range, SZ patients showed less fraction of time in
557 the FPN-DMN state (State 1 and 2) and more in the SN-DMN state (State 3 and 4) in
558 both slow-4 and slow-5. The FPN, DMN and SN have been widely reported abnormal
559 in psychiatric disorders as triple-network model (Manoliu et al. 2014; Menon 2011;
560 Supekar et al. 2019), and our results further showed the altered triple-network
561 dynamics in SZ patients exist in both slow-4 and slow-5. Besides, frequency-specific
562 alterations were also found between slow-4 and slow-5. Particularly significant group-
563 frequency interactions in the SN-DMN state were obtained on all the three CAP
564 dynamics (fraction of time, persistence and counts), and increased persistence in the
565 SN-DMN state was only obtained in slow-5 but not in slow-4 nor the typical range.
566 The reason might be that slow-5 was characterized by stronger DMN activation
567 deviation in the SN-DMN state, and the more active spatial foundation provides richer
568 temporal dynamics, enabling the discovery of more distinguished disease alterations.
569 Furthermore, combining the features from both slow-4 and slow-5 have increased the
570 diagnose accuracy of schizophrenia patients than only use the typical range. Previous
571 studies have also shown the increased classification accuracy by combing slow-4 and
572 slow-5 (Huang et al. 2019; Tian et al. 2020). Together, these results suggest that
573 frequency-dependent dynamic information contains in multi-frequency bands, and
574 could help to identify frequency-specific disease alterations.

575

576 **4.4 Limitations**

577 In this study, we used frequency divisions from slow-5 to slow-2 as was
578 described by Buzsaki (Buzsaki and Draguhn 2004) and used by Zuo and colleagues
579 (Zuo et al. 2010) in fMRI. Although, this method has been widely adapted in fMRI
580 that uses unequal ranges of frequency bandwidths, recent studies have shown a

581 wavelet-based method with higher sensitivity and reproducibility to obtain the sub-
582 frequency bands (Luo, Wang, et al. 2020). Future studies should validate and compare
583 the frequency-dependent CAPs obtained by wavelet transform and fast Fourier
584 transform. Besides, the effects of physiological noises such as head movement,
585 cardiac and respiratory motion were not fully studied. Although, subjects with large
586 headmotion were excluded before the analysis, and the 24 headmotion parameters
587 (Friston et al. 1996) were regressed from the BOLD signal, headmotion could still
588 affect the dynamic functional connectivity (Nalci, Rao, and Liu 2019; Laumann et al.
589 2017). Whether and how the headmotion would influence the spatial and temporal
590 characteristics of CAPs remains further study. The cardiac and respiratory motions
591 were not recorded during the scan, and have not been corrected from the time series
592 using methods such as RETROICOR (Glover, Li, and Ress 2000). While slow-3 and
593 slow-2 might be involved with these high-frequency noises, hence their effects on
594 CAPs cannot be studied systematically in current work.

595

596 **5. Conclusions**

597 This study proved that the resting-state CAP states showed frequency-specific
598 spatial and temporal characteristics. In summary, from slow-5 to slow-2, the spatial
599 patterns varied from intrinsic functional networks to irregular configurations, and the
600 CAP state became more unstable and frequently changed when the frequency band
601 increased, which caused shorter persistence and more counts. Besides, our results
602 supported that, the large-scale network integration relies more on lower-frequency
603 oscillations (slow-5) and the subcortical regions activate more in a relative higher-
604 frequency band (slow-4), from a dynamic point of view. Finally, frequency-dependent
605 dynamic changes in schizophrenia patients were also observed between slow-5 and
606 slow-4. Our results could provide more information about the functional dynamic
607 brain, and help to understand the frequency-specific pathological mechanisms of
608 psychiatric disorders.

609

610 **Conflict of interest**

611 The authors declare no conflict of interest.

612

613 **Data and code availability statements**

614 The data used in this study is not publicly available due to privacy or ethical restrictions.

615 The code that supports the findings of this study will be made available upon request

616 from the corresponding author.

617

618 **Acknowledgements**

619 We are grateful to all the patients and volunteers of this study as well as the staffs at the

620 Wuxi Mental Health Center for their help with participant recruitment and data

621 collection. This work was supported by the National Natural Science Foundation of

622 China (NSFC) grant (No. 62071109 to C.M., No. 81871081 and 81301148 to L.T., No.

623 61871420 to B.B.),

624

625 **References**

- 626 Allen, E. A., E. Damaraju, S. M. Plis, E. B. Erhardt, T. Eichele, and V. D. Calhoun. 2014. 'Tracking
627 Whole-Brain Connectivity Dynamics in the Resting State', *Cerebral Cortex*, 24: 663-76.
- 628 Biswal, B., F. Z. Yetkin, V. M. Haughton, and J. S. Hyde. 1995. 'Functional Connectivity in the
629 Motor Cortex of Resting Human Brain Using Echo-Planar Mri', *Magnetic Resonance in
630 Medicine*, 34: 537-41.
- 631 Buzsaki, G., and A. Draguhn. 2004. 'Neuronal oscillations in cortical networks', *Science*, 304: 1926-
632 9.
- 633 Chang, C., and G. H. Glover. 2010. 'Time-frequency dynamics of resting-state brain connectivity
634 measured with fMRI', *Neuroimage*, 50: 81-98.
- 635 Chen, J. E., and G. H. Glover. 2015. 'BOLD fractional contribution to resting-state functional
636 connectivity above 0.1 Hz', *Neuroimage*, 107: 207-18.
- 637 Cordes, D., V. M. Haughton, K. Arfanakis, J. D. Carew, P. A. Turski, C. H. Moritz, M. A. Quigley,
638 and M. E. Meyerand. 2001. 'Frequencies contributing to functional connectivity in the
639 cerebral cortex in "resting-state" data', *AJNR Am J Neuroradiol*, 22: 1326-33.
- 640 Damaraju, E., E. A. Allen, A. Belger, J. M. Ford, S. McEwen, D. H. Mathalon, B. A. Mueller, G. D.
641 Pearlson, S. G. Potkin, A. Preda, J. A. Turner, J. G. Vaidya, T. G. van Erp, and V. D. Calhoun.
642 2014. 'Dynamic functional connectivity analysis reveals transient states of dysconnectivity
643 in schizophrenia', *Neuroimage Clin*, 5: 298-308.
- 644 Di, X., and B. B. Biswal. 2015. 'Characterizations of resting-state modulatory interactions in the
645 human brain', *J Neurophysiol*, 114: 2785-96.
- 646 Du, Y. H., G. D. Pearlson, D. D. Lin, J. Sui, J. Y. Chen, M. Salman, C. A. Tamminga, E. I. Ivleva, J.
647 A. Sweeney, M. S. Keshavan, B. A. Clementz, J. Bustillo, and V. D. Calhoun. 2017.
648 'Identifying Dynamic Functional Connectivity Biomarkers Using GIG-ICA: Application to
649 Schizophrenia, Schizoaffective Disorder, and Psychotic Bipolar Disorder', *Human brain
650 mapping*, 38: 2683-708.
- 651 Friston, K. J., S. Williams, R. Howard, R. S. Frackowiak, and R. Turner. 1996. 'Movement-related
652 effects in fMRI time-series', *Magn Reson Med*, 35: 346-55.
- 653 Glover, G. H., T. Q. Li, and D. Ress. 2000. 'Image-based method for retrospective correction of
654 physiological motion effects in fMRI: RETROICOR', *Magn Reson Med*, 44: 162-7.
- 655 Gohel, S., J. A. Gallego, D. G. Robinson, P. DeRosse, B. Biswal, and P. R. Szeszko. 2018.
656 'Frequency specific resting state functional abnormalities in psychosis', *Hum Brain Mapp*,
657 39: 4509-18.
- 658 Gohel, Suril R, and Bharat B %J Brain connectivity Biswal. 2015. 'Functional integration between
659 brain regions at rest occurs in multiple-frequency bands', 5: 23-34.
- 660 Guo, X. N., X. J. Duan, J. Suckling, H. Chen, W. Liao, Q. Cui, and H. F. Chen. 2019. 'Partially
661 impaired functional connectivity states between right anterior insula and default mode
662 network in autism spectrum disorder', *Human brain mapping*, 40: 1264-75.
- 663 Han, S., X. Zong, M. Hu, Y. Yu, X. Wang, Z. Long, Y. Wang, X. Chen, and H. Chen. 2017.
664 'Frequency-selective alteration in the resting-state corticostriatal-thalamo-cortical circuit
665 correlates with symptoms severity in first-episode drug-naive patients with schizophrenia',
666 *Schizophrenia Research*, 189: 175-80.
- 667 Han, Y., J. Wang, Z. Zhao, B. Min, J. Lu, K. Li, Y. He, and J. Jia. 2011. 'Frequency-dependent
668 changes in the amplitude of low-frequency fluctuations in amnesic mild cognitive

- 669 impairment: a resting-state fMRI study', *Neuroimage*, 55: 287-95.
- 670 Hare, S. M., J. M. Ford, A. Ahmadi, E. Damaraju, A. Belger, J. Bustillo, H. J. Lee, D. H. Mathalon,
671 B. A. Mueller, A. Preda, T. G. van Erp, S. G. Potkin, V. D. Calhoun, J. A. Turner, and
672 Network Functional Imaging Biomedical Informatics Research. 2017. 'Modality-
673 Dependent Impact of Hallucinations on Low-Frequency Fluctuations in Schizophrenia',
674 *Schizophr Bull*, 43: 389-96.
- 675 Hou, Y., X. Wu, M. Hallett, P. Chan, and T. Wu. 2014. 'Frequency-dependent neural activity in
676 Parkinson's disease', *Hum Brain Mapp*, 35: 5815-33.
- 677 Huang, J., Q. Zhu, X. Hao, X. Shi, S. Gao, X. Xu, and D. Zhang. 2019. 'Identifying Resting-State
678 Multifrequency Biomarkers via Tree-Guided Group Sparse Learning for Schizophrenia
679 Classification', *IEEE J Biomed Health Inform*, 23: 342-50.
- 680 Huang, Z., J. Zhang, J. Wu, G. A. Mashour, and A. G. Hudetz. 2020. 'Temporal circuit of macroscale
681 dynamic brain activity supports human consciousness', *Sci Adv*, 6: eaaz0087.
- 682 Hutchison, R. M., T. Womelsdorf, E. A. Allen, P. A. Bandettini, V. D. Calhoun, M. Corbetta, S.
683 Penna, J. H. Duyn, G. H. Glover, J. Gonzalez-Castillo, D. A. Handwerker, S. Keilholz, V.
684 Kiviniemi, D. A. Leopold, F. Pasquale, O. Sporns, M. Walter, and C. Chang. 2013.
685 'Dynamic functional connectivity: Promise, issues, and interpretations', *Neuroimage*, 80:
686 360-78.
- 687 Kaiser, R. H., M. S. Kang, Y. Lew, J. Van Der Feen, B. Aguirre, R. Clegg, F. Goer, E. Esposito, R.
688 P. Auerbach, R. M. Hutchison, and D. A. Pizzagalli. 2019. 'Abnormal frontoinsula-default
689 network dynamics in adolescent depression and rumination: a preliminary resting-state co-
690 activation pattern analysis', *Neuropsychopharmacology*, 44: 1604-12.
- 691 Kottaram, A., L. Johnston, E. Ganella, C. Pantelis, R. Kotagiri, and A. Zalesky. 2018. 'Spatio-
692 temporal dynamics of resting-state brain networks improve single-subject prediction of
693 schizophrenia diagnosis', *Hum Brain Mapp*, 39: 3663-81.
- 694 Laumann, T. O., A. Z. Snyder, A. Mitra, E. M. Gordon, C. Gratton, B. A. Yeo, A. W. Gilmore, S.
695 M. Nelson, J. J. Berg, D. J. Greene, J. E. McCarthy, E. Tagliazucchi, H. Laufs, B. L.
696 Schlaggar, N. U. F. Dosenbach, and S. E. Petersen. 2017. 'On the Stability of BOLD fMRI
697 Correlations', *Cereb Cortex*, 27: 4719-32.
- 698 Li, C., M. S. Dong, F. Y. Womer, S. Q. Han, Y. Yin, X. W. Jiang, Y. E. Wei, J. Duan, R. Q. Feng, L.
699 H. Zhang, X. Z. Zhang, F. Wang, Y. Q. Tang, and K. Xu. 2020. 'Transdiagnostic time-
700 varying dysconnectivity across major psychiatric disorders', *Human brain mapping*.
- 701 Li, M., L. Dahmani, D. Wang, J. Ren, S. Stocklein, Y. Lin, G. Luan, Z. Zhang, G. Lu, F. Galie, Y.
702 Han, A. Pascual-Leone, M. Wang, M. D. Fox, and H. Liu. 2020. 'Co-activation patterns
703 across multiple tasks reveal robust anti-correlated functional networks', *Neuroimage*, 227:
704 117680.
- 705 Liu, X., C. Chang, and J. H. Duyn. 2013. 'Decomposition of spontaneous brain activity into distinct
706 fMRI co-activation patterns', *Front Syst Neurosci*, 7: 101.
- 707 Liu, X., and J. H. Duyn. 2013. 'Time-varying functional network information extracted from brief
708 instances of spontaneous brain activity', *Proc Natl Acad Sci U S A*, 110: 4392-7.
- 709 Luo, F. F., J. B. Wang, L. X. Yuan, Z. W. Zhou, H. Xu, S. H. Ma, Y. F. Zang, and M. Zhang. 2020.
710 'Higher Sensitivity and Reproducibility of Wavelet-Based Amplitude of Resting-State
711 fMRI', *Front Neurosci*, 14: 224.
- 712 Luo, Y. L., H. He, M. J. Duan, H. Huang, Z. F. Hu, H. M. Wang, G. Yao, D. Z. Yao, J. F. Li, and C.

- 713 Luo. 2020. 'Dynamic Functional Connectivity Strength Within Different Frequency-Band
714 in Schizophrenia', *Frontiers in Psychiatry*, 10.
- 715 Ma, X., Z. Zhuo, L. Wei, Z. Ma, Z. Li, H. Li, and Initiative Alzheimer's Disease Neuroimaging.
716 2020. 'Altered Temporal Organization of Brief Spontaneous Brain Activities in Patients
717 with Alzheimer's Disease', *Neuroscience*, 425: 1-11.
- 718 Manoliu, A., V. Riedl, A. Zherdin, M. Muhlau, D. Schwerthoffer, M. Scherr, H. Peters, C. Zimmer,
719 H. Forstl, J. Bauml, A. M. Wohlschlagel, and C. Sorg. 2014. 'Aberrant dependence of
720 default mode/central executive network interactions on anterior insular salience network
721 activity in schizophrenia', *Schizophr Bull*, 40: 428-37.
- 722 Marusak, H. A., V. D. Calhoun, S. Brown, L. M. Crespo, K. Sala-Hamrick, I. H. Gotlib, and M. E.
723 Thomason. 2017. 'Dynamic functional connectivity of neurocognitive networks in children',
724 *Hum Brain Mapp*, 38: 97-108.
- 725 Meda, S. A., Z. Wang, E. I. Ivleva, G. Poudyal, M. S. Keshavan, C. A. Tamminga, J. A. Sweeney,
726 B. A. Clementz, D. J. Schretlen, V. D. Calhoun, S. Lui, E. Damaraju, and G. D. Pearlson.
727 2015. 'Frequency-Specific Neural Signatures of Spontaneous Low-Frequency Resting State
728 Fluctuations in Psychosis: Evidence From Bipolar-Schizophrenia Network on Intermediate
729 Phenotypes (B-SNIP) Consortium', *Schizophr Bull*, 41: 1336-48.
- 730 Menon, V. 2011. 'Large-scale brain networks and psychopathology: a unifying triple network model',
731 *Trends Cogn Sci*, 15: 483-506.
- 732 Nalci, A., B. D. Rao, and T. T. Liu. 2019. 'Nuisance effects and the limitations of nuisance regression
733 in dynamic functional connectivity fMRI', *Neuroimage*, 184: 1005-31.
- 734 Penttonen, Markku, György %J Thalamus Buzsáki, and Related Systems. 2003. 'Natural logarithmic
735 relationship between brain oscillators', 2: 145-52.
- 736 Reinen, J. M., O. Y. Chen, R. M. Hutchison, B. T. T. Yeo, K. M. Anderson, M. R. Sabuncu, D. Ongur,
737 J. L. Roffman, J. W. Smoller, J. T. Baker, and A. J. Holmes. 2018. 'The human cortex
738 possesses a reconfigurable dynamic network architecture that is disrupted in psychosis',
739 *Nature Communications*, 9.
- 740 Rousseeuw, P. J. 1987. 'Silhouettes: a graphical aid to the interpretation and validation of cluster
741 analysis', *Journal of Computational and Applied Mathematics*, 20: 53-65.
- 742 Salvador, R., J. Suckling, C. Schwarzbauer, and E. Bullmore. 2005. 'Undirected graphs of
743 frequency-dependent functional connectivity in whole brain networks', *Philos Trans R Soc
744 Lond B Biol Sci*, 360: 937-46.
- 745 Schaefer, A., R. Kong, E. M. Gordon, T. O. Laumann, X. N. Zuo, A. J. Holmes, S. B. Eickhoff, and
746 B. T. T. Yeo. 2018. 'Local-Global Parcellation of the Human Cerebral Cortex from Intrinsic
747 Functional Connectivity MRI', *Cereb Cortex*, 28: 3095-114.
- 748 Shakil, S., C. H. Lee, and S. D. Keilholz. 2016. 'Evaluation of sliding window correlation
749 performance for characterizing dynamic functional connectivity and brain states',
750 *Neuroimage*, 133: 111-28.
- 751 Supekar, K., W. Cai, R. Krishnadas, L. Palaniyappan, and V. Menon. 2019. 'Dysregulated Brain
752 Dynamics in a Triple-Network Saliency Model of Schizophrenia and Its Relation to
753 Psychosis', *Biol Psychiatry*, 85: 60-69.
- 754 Tian, Z. Y., L. Qian, L. Fang, X. H. Peng, X. H. Zhu, M. Wu, W. Z. Wang, W. H. Zhang, B. Q. Zhu,
755 M. Wan, X. Hu, and J. B. Shao. 2020. 'Frequency-Specific Changes of Resting Brain
756 Activity in Parkinson's Disease: A Machine Learning Approach', *Neuroscience*, 436: 170-

- 757 83.
- 758 Tzourio-Mazoyer, N., B. Landeau, D. Papathanassiou, F. Crivello, O. Etard, N. Delcroix, B.
759 Mazoyer, and M. Joliot. 2002. 'Automated anatomical labeling of activations in SPM using
760 a macroscopic anatomical parcellation of the MNI MRI single-subject brain', *Neuroimage*,
761 15: 273-89.
- 762 Wang, C. H., J. L. Ong, A. Patanaik, J. Zhou, and M. W. L. Chee. 2016. 'Spontaneous eyelid closures
763 link vigilance fluctuation with fMRI dynamic connectivity states', *Proceedings of the
764 National Academy of Sciences of the United States of America*, 113: 9653-58.
- 765 Wang, L., Q. Kong, K. Li, Y. Su, Y. Zeng, Q. Zhang, W. Dai, M. Xia, G. Wang, Z. Jin, X. Yu, and T.
766 Si. 2016. 'Frequency-dependent changes in amplitude of low-frequency oscillations in
767 depression: A resting-state fMRI study', *Neurosci Lett*, 614: 105-11.
- 768 Wang, X., Y. Zhang, Z. Long, J. Zheng, Y. Zhang, S. Han, Y. Wang, X. Duan, M. Yang, J. Zhao, and
769 H. Chen. 2017. 'Frequency-specific alteration of functional connectivity density in
770 antipsychotic-naive adolescents with early-onset schizophrenia', *J Psychiatr Res*, 95: 68-
771 75.
- 772 Weng, Y., X. Liu, H. Hu, H. Huang, S. Zheng, Q. Chen, J. Song, B. Cao, J. Wang, S. Wang, and R.
773 Huang. 2020. 'Open eyes and closed eyes elicit different temporal properties of brain
774 functional networks', *Neuroimage*, 222: 117230.
- 775 Xue, S. W., D. Li, X. C. Weng, G. Northoff, and D. W. Li. 2014. 'Different neural manifestations of
776 two slow frequency bands in resting functional magnetic resonance imaging: a systemic
777 survey at regional, interregional, and network levels', *Brain Connect*, 4: 242-55.
- 778 Yang, H., H. Zhang, X. Di, S. Wang, C. Meng, L. Tian, and B. Biswal. 2021. 'Reproducible
779 Coactivation Patterns of Functional Brain Networks Reveal the Aberrant Dynamic State
780 Transition in Schizophrenia', *Neuroimage*: 118193.
- 781 Yang, Hang, Xin Di, Qiyong Gong, John Sweeney, Bharat %J Brain Structure Biswal, and Function.
782 2020. 'Investigating inhibition deficit in schizophrenia using task-modulated brain
783 networks', 225: 1601-13.
- 784 Yu, Q., E. B. Erhardt, J. Sui, Y. Du, H. He, D. Hjelm, M. S. Cetin, S. Rachakonda, R. L. Miller, G.
785 Pearlson, and V. D. Calhoun. 2015. 'Assessing dynamic brain graphs of time-varying
786 connectivity in fMRI data: application to healthy controls and patients with schizophrenia',
787 *Neuroimage*, 107: 345-55.
- 788 Yu, R., Y. L. Chien, H. L. Wang, C. M. Liu, C. C. Liu, T. J. Hwang, M. H. Hsieh, H. G. Hwu, and
789 W. Y. Tseng. 2014. 'Frequency-specific alternations in the amplitude of low-frequency
790 fluctuations in schizophrenia', *Hum Brain Mapp*, 35: 627-37.
- 791 Yu, R., M. H. Hsieh, H. L. Wang, C. M. Liu, C. C. Liu, T. J. Hwang, Y. L. Chien, H. G. Hwu, and
792 W. Y. Tseng. 2013. 'Frequency dependent alterations in regional homogeneity of baseline
793 brain activity in schizophrenia', *Plos One*, 8: e57516.
- 794 Yu, X. Y., B. K. Yuan, Q. J. Cao, L. An, P. Wang, A. Vance, T. J. Silk, Y. F. Zang, Y. F. Wang, and L.
795 Sun. 2016. 'Frequency-specific abnormalities in regional homogeneity among children with
796 attention deficit hyperactivity disorder: a resting-state fMRI study', *Science Bulletin*, 61:
797 682-92.
- 798 Zalesky, A., and M. Breakspear. 2015. 'Towards a statistical test for functional connectivity
799 dynamics', *Neuroimage*, 114: 466-70.
- 800 Zhang, J., Z. Huang, S. Tumati, and G. Northoff. 2020. 'Rest-task modulation of fMRI-derived

801 global signal topography is mediated by transient coactivation patterns', *PLoS Biol*, 18:
802 e3000733.
803 Zhang, Y., R. Yang, and X. Cai. 2020. 'Frequency-specific alternations in the moment-to-moment
804 BOLD signals variability in schizophrenia', *Brain Imaging Behav*.
805 Zou, H. L., and J. Yang. 2019. 'Multi-frequency Dynamic Weighted Functional Connectivity
806 Networks for Schizophrenia Diagnosis', *Applied Magnetic Resonance*, 50: 847-59.
807 Zuo, X. N., A. Di Martino, C. Kelly, Z. E. Shehzad, D. G. Gee, D. F. Klein, F. X. Castellanos, B. B.
808 Biswal, and M. P. Milham. 2010. 'The oscillating brain: complex and reliable', *Neuroimage*,
809 49: 1432-45.
810